RSC Advances

REVIEW

View Article Online
View Journal | View Issue

Cite this: *RSC Adv.*, 2022, **12**, 19512

Synthesis of MoS_2-based nanostructures and their applications in rechargeable ion batteries, catalysts and gas sensors: a review

Wei Sun, [ac] Yaofang Zhang,*[ac] Weimin Kang, [ad] Nanping Deng,[ad] Xiaoxiao Wang,[ad] Xiaoying Kang,[ac] Zirui Yan,[ac] Yingwen Pan[ac] and Jian Ni[b]

Received 8th March 2022
Accepted 17th June 2022

DOI: 10.1039/d2ra01532c

rsc.li/rsc-advances

Molybdenum disulfide (MoS_2) is a two-dimensional (2D) layered material with a graphene-like structure that has attracted attention because of its large specific surface area and abundant active sites. In addition, the compounding of MoS_2 with other materials can enhance the performance in applications such as batteries, catalysts, and optoelectronic devices, *etc.* MoS_2 is prepared by various methods, among which chemical deposition and hydrothermal methods are widely used. In this review, we focus on summarizing the applications of MoS_2 and MoS_2 composite nanomaterials in rechargeable ion batteries, catalysts for water splitting and gas sensors, and briefly outline the preparation methods.

1. Introduction

Nanomaterials have attracted increasing research interest as a result of its fascinating physicochemical properties, such as the nano-size effect and large specific surface area. In 2005, the emergence of monolayer graphene set off a research boom in 2D materials.[1–3] Many novel 2D materials have also been developed, such as hexagonal boron nitride (hBN) and transition metal dichalcogenides (TMDs). They are widely used in energy, sensing and other applications due to their excellent physical and chemical properties.[4–9] Notably, MoS_2, a member of TMDs, is a promising 2D material among compounds with graphene-like structures.

It is well known that MoS_2 materials have a wide range of applications, and we found that it has a high proportion of catalysts, batteries and gas sensors applications by searching the Web of Science for articles related to the applications of MoS_2 in the last decade (Fig. 1b). Fig. 1a summarizes the number of published SCI papers on MoS_2 over the last decade (up to May 2022) in the batteries, catalysts, and gas sensors. It is clear that MoS_2 is attracting more and more attention in these applications.

MoS_2 exhibits unique advantages over graphene-based or hBN-based nanomaterials in these applications. In detail, in batteries, MoS_2 is used as an electrode material due to its high specific surface area and unique layer-like structure.[10] In catalysts, MoS_2 is a promising alternative to the precious metal Pt catalysts for hydrogen reaction evolution (HER) and

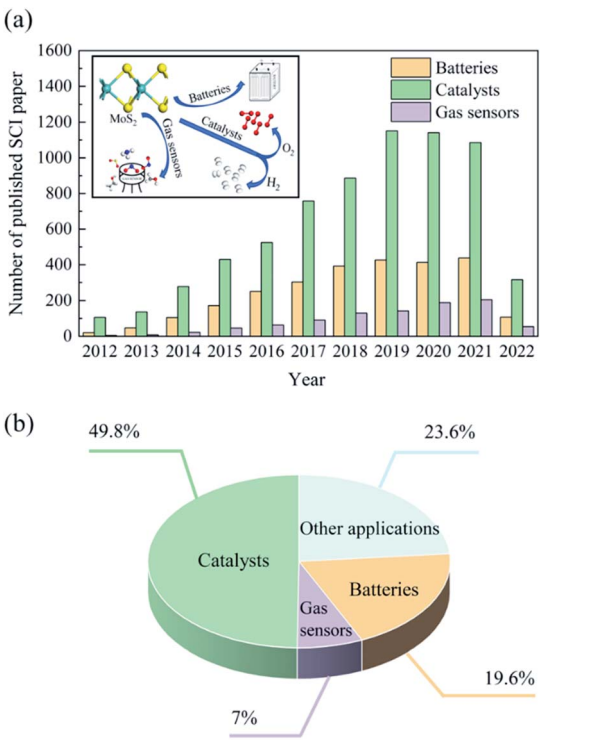

Fig. 1 (a) Statistics of MoS_2 core publications in batteries, catalysts, and gas sensors. (b) Percentage of core publications of MoS_2 in different applications in the last decade (up to May 2022).

[a]State Key Laboratory of Separation Membranes and Membrane Processes, Tiangong University, Tianjin 300387, PR China
[b]Department of Electronic Science and Technology, College of Electronic Information and Optical Engineering, Nankai University, Tianjin, 300350, China
[c]School of Physical Science and Technology, Tiangong University, Tianjin 300387, PR China
[d]School of Textile Science and Engineering, Tiangong University, Tianjin 300387, China

photocatalytic water splitting, while MoS_2 can be used in combination with other materials to improve visible light catalytic activity for the degradation of organic pollutants in industrial wastewater.[11,12] In terms of gas-sensitive properties, MoS_2 has good responsiveness and selectivity to some gases at room temperature (RT), which has led to widespread research and application of MoS_2 materials in gas sensors.[13]

Recent years, many reviews about MoS_2 nanomaterials were published. Some researchers have reviewed the application and preparation of MoS_2 in energy (such as batteries and catalysts),[14–16] some have reviewed the application and preparation of MoS_2 in electronic components (such as memristors and field-effect transistors),[17–20] some focus on MoS_2 for detection and sensing applications,[21–23] some have listed in detail the synthesis and application of 1T MoS_2,[24–26] and others have focused on the synthesis method of MoS_2.[27] Based on the previous researches and summaries, in this review, we comprehensively and systematically describe the applications of MoS_2 and MoS_2-based composites in rechargeable ion batteries, catalysts and gas sensors in recent years, and summarize the corresponding preparation schemes.

2. Applications and synthesis strategies of MoS_2 in rechargeable ion batteries

To meet future energy storage needs, rechargeable ion batteries based on Li^+, Na^+, Al^{3+} and Zn^{2+} have been widely studied and prepared.[28–31] MoS_2 has a layered structure, which are connected by van der Waals forces with weak interlayer interactions and large layer spacing.[32] High theoretical capacity, high charging rate and excellent stability make MoS_2 become a promising electrode material. In this work, we will focus on the application and preparation of MoS_2 as electrode materials.

2.1 Lithium-ion batteries

Using MoS_2 or composites of MoS_2 for the anode materials is beneficial to lithium-ion batteries (LIBs). Wei *et al.*[33] studied the electrochemical reactions of MoS_2 nanosheets in LIBs. Their study represented that intercalation of Li ions into MoS_2 anode contributes the electrochemical charge storage. However, the low conductive of MoS_2 and its aggregation during the electrode manufacturing process greatly hinder the development of LIBs.[34,35] In order to improve the performance of MoS_2 as an electrode material for LIBs, there are two main options, one is to change the structure of MoS_2 material, and the other is to prepare MoS_2 composites.

On the one hand, Zhao *et al.*[36] studied MoS_2 materials with nanotube structures to improve electrochemical performance. They reported a facile wet etching method for the preparation of low crystalline MoS_2 nanotubes. First, MoO_3 nanobelts (MoO_3 NBs) were prepared by hydrothermal method. Sodium molybdate dihydrate ($Na_2MoO_4 \cdot 2H_2O$) and nitric acid were used in this step. Second, 3D MoS_2 nanomasks were grown *in situ* on MoO_3 NBs, which was obtained by the chemical reaction of sublimed sulfur with MoO_3 NBs in CVD quartz tube. Finally, MoS_2 nanotubes (MoS_2 NTs) were synthesized by mixing the previously obtained MoO_x/MoS_2 NBs with concentrated hydrochloric acid. As demonstrated in Fig. 2a, the inner MoO_x are etched with concentrated hydrochloric acids to yield low crystalline MoS_2 NTs. With the increase of etching times, the molybdenum oxide is gradually removed which allowed the internal cavity of MoS_2 NTs to be emptied. After the fourth etching process, most of the molybdenum oxides were removed to give MoS_2 NTs (Fig. 2b).

The electrochemical test results illustrated that MoS_2 NTs, as the anode material for LIBs, reached a specific capacity of 1253 mA g^{-1} at a current rate of 200 mA g^{-1} and was stabilized after 250 cycles. Obviously, the low crystalline MoS_2 NTs have even higher specific capacity and cyclic performance than the reported electrode materials.[37,38]

On the other hand, some researchers have investigated MoS_2 nanocomposites to improve the electrochemical properties of MoS_2 in LIBs.

Wu *et al.*[34] reported an electrode material of two-layer carbon-coated MoS_2/carbon nanofiber (MoS_2/C/C fiber) which prepared by hydrothermal and electrospinning method. First, MoS_2 spheres were obtained by hydrothermal. Hexaammonium heptamolybdate tetrahydrate ($(NH_4)_6Mo_7O_{24} \cdot 4H_2O$), thiourea ($NH_2CSNH_2$), and polyvinylpyrrolidone (PVP) were used in this step. Second, MoS_2/C spheres were fabricated by using glucose and the above-obtained MoS_2 spheres. Finally, they synthesized MoS_2/C/C nanofiber by electrospinning method. Polyacrylonitrile (PAN), *N*,*N*-dimethylformamide (DMF) and the above obtained MoS_2/C spheres were used. The preparation process of MoS_2/C/C fiber is shown in Fig. 2c.

Meanwhile, Zhang *et al.*[35] synthesized TiO_2/C/MoS_2 microspheres as anodes for LIBs. TiO_2/C/MoS_2 microspheres were prepared by solvent-thermal method and calcination. First of all they used PVP, acetic acid and tetrabutyltitanate (TBT) in a Teflon-lined autoclave for the reaction to prepare TiO_2/C materials. Secondly, TiO_2/C/MoS_2 was synthesized by the obtained TiO_2/C, ammonium molybdatetetrahydrate ($(NH_4)_6Mo_7O_{24} \cdot 4H_2O$) and thiourea ($CH_4N_2S$). The preparation process of TiO_2/C/MoS_2 microsphere is shown in Fig. 2e.

No matter MoS_2 is compounded with carbon materials or TiO_2 materials, the electrochemical properties of MoS_2 materials have been improved. On the one hand, for the MoS_2/C/C electrode, the double-layer carbon coating (Fig. 2d) could not only suppress the irreversible reaction, but also confine the volume change during the lithiation/delithiation process.[34] Moreover, MoS_2/C/C fiber has better cycling performance than MoS_2 spheres (Fig. 2g). On the other hand, the unique structure with flower-shaped of TiO_2/C/MoS_2 (Fig. 2f) could not only enlarge the electrolyte–electrode interface area but also shorten the diffusion length of Li^+ intercalation/deintercalation.[35] Compared with MoS_2 materials, the cycling performance of TiO_2/C/MoS_2 are enhanced (Fig. 2h).

2.2 Sodium-ion batteries

Sodium ion batteries (SIBs) are considered as an alternative to LIBs because of their abundant reserves and low cost. However,

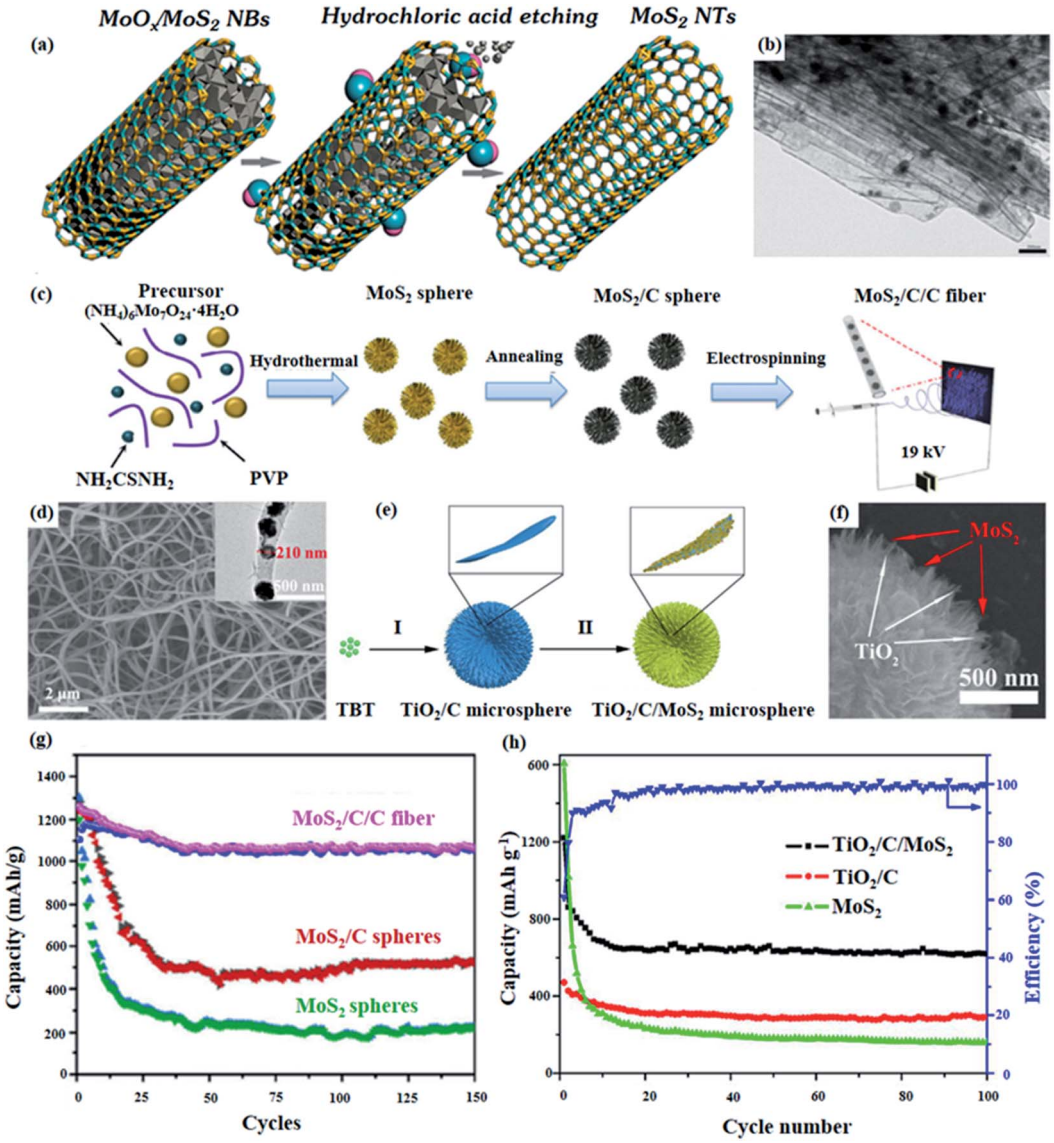

Fig. 2 (a) MoS_2 NTs are obtained after etching MoO_x/MoS_2 NBs with concentrated hydrochloric acid.[36] (b) MoS_2 NTs obtained from the fourth etching.[36] (c) Schematic illustration of the preparation process of MoS_2/C/C fiber.[34] (d) SEM images of MoS_2/C/C fiber. The inset is a magnified TEM image of the sample.[34] (e) Schematic diagram of the synthesis of TiO_2/C/MoS_2 microsphere.[35] (f) SEM images of TiO_2/C/MoS_2 microsphere.[35] (g) Capacity retention of the MoS_2, MoS_2/C, and MoS_2/C/C fiber electrodes at a current density of 0.2 A g^{-1} for the subsequent 150 cycles.[36] (h) Comparative cycling performance of MoS_2, TiO_2/C and the TiO_2/C/MoS_2 microsphere at a current density of 100 mA g^{-1}.[35]

Na^+ has larger radius than Li^+,[39] which hingers the development of SIBs. As a highly promising electrode material, MoS_2 has not only a layered structure but also a large interlayer spacing, which promises to solve the inherent defects of SIBs. However, MoS_2 also has inherent limitations, such as low intrinsic electron conductivity. In response to these characteristics, some researchers have prepared composites of MoS_2 [40–43] and others have improved the structure of MoS_2 by doping or inserting molecules to achieve improved electrochemical properties.[40–45]

Pan *et al.*[42] reported a simple template method to prepared MoS_2/amorphous carbon (C) microtubes (MTs) composed of heterostructured MoS_2/C nanosheets. The synthesis of MoS_2/C MTs was achieved by a three-step procedure: first, obtaining Sb_2S_3 microrods by a simple hydrothermal method, second, MoS_2/C nanosheets were grown on the outer surface of Sb_2S_3 microrods by using sodium molybdate dehydrate ($Na_2MoO_4 \cdot 2H_2O$), N_2H_4CS, and glucose ($C_6H_{12}O_6$) in a Teflon-lined stainless steel autoclave for chemical reaction, and third, MoS_2/C MTs were obtained by removing Sb_2S_3 microrods *via* annealing. The synthesis schematic is shown in Fig. 3a. Electrochemical measurements demonstrated that MoS_2/C MTs possessed high specific capacity and excellent stability, improving the electrochemical performance of SIBs.

Similarly, some researchers have also reported composites of MoS_2 for enhancing the electrochemical performance of SIBs.

The MoS_2/carbon nanofibers (MoS_2/CNFs) were prepared by a two-step procedures: first, obtaining ammonium tetrathiomolybdate (AMT), and second, synthesizing MoS_2/CNFs by

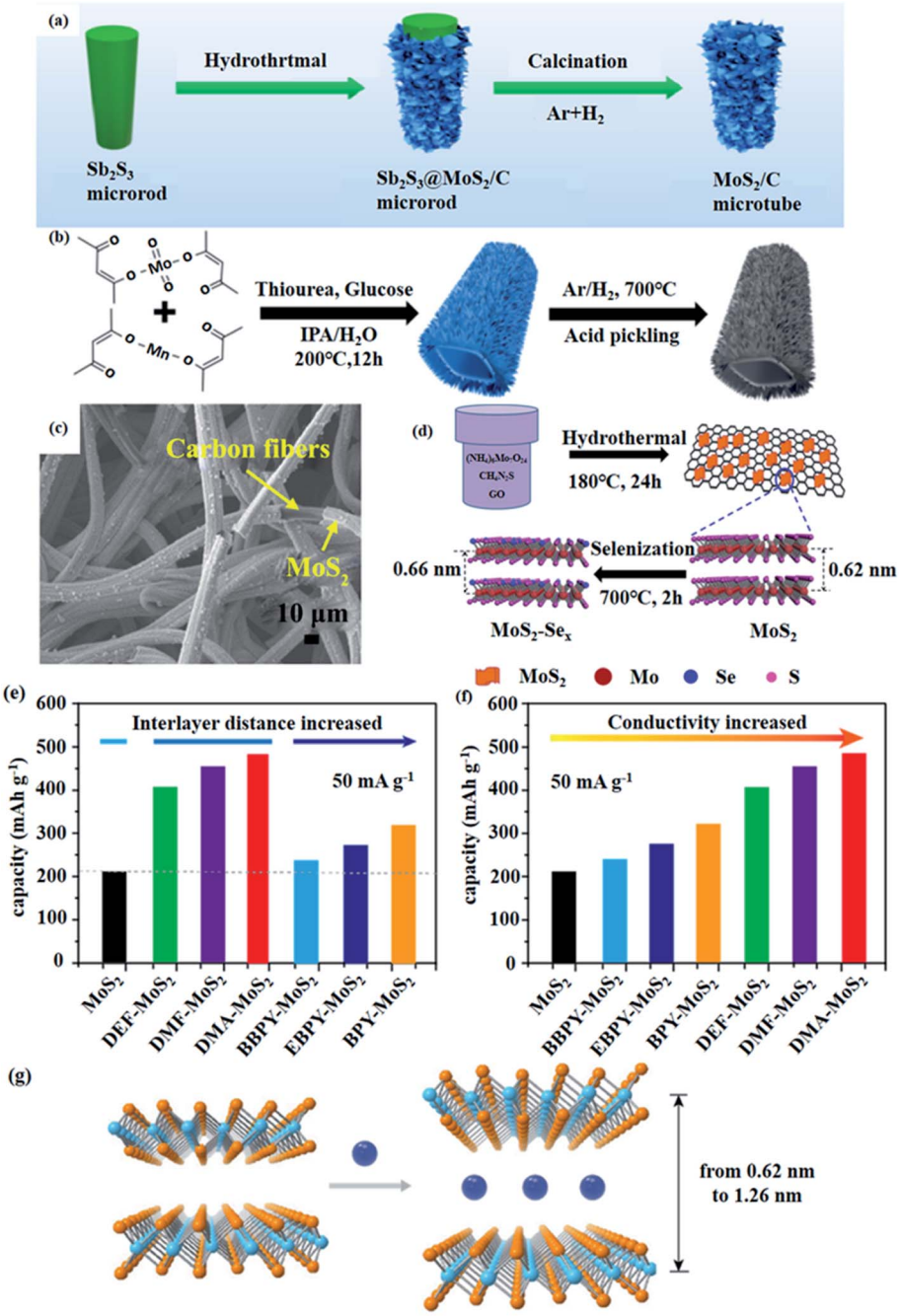

Fig. 3 (a) Schematic illustration of the synthesis process of MoS_2/C MTs.[42] (b) Schematic diagram of the fabrication process of MoS_2–C hollow rhomboids.[41] (c) FESEM images of OMSCF calcined in air at 400 °C (OMSCF-400).[43] (d) Schematic illustration of the synthesis of $MoS_{2-x}Se_x$/G.[45] (e) Capacity of all intercalated MoS_2 at 50 mA g^{-1} arranged according to the interlayer distance, respectively.[44] (f) Capacity of all intercalated MoS_2 50 mA g^{-1} arranged according to conductivity, respectively.[44] (g) Schematic of intercalation of molecules into MoS_2.[44]

electrospinning and high temperature carbonization. MoS_2/CNFs have a large specific surface area and high electrical conductivity, which enhances Na storage performance.[40]

The MoS_2–C hollow rhomboids (MCHRs) were fabricated by a sample one-pot solvothermal reaction (Fig. 3b). First of all, manganese(II)acetylacetonate ($Mn(acac)_2$), molybdenyl acetylacetonate ($MoO_2(acac)_2$) were dispersed in distilled water and isopropanol. And then, glucose and thiourea were incorporated into the mixture. Finally, the mixture was annealed after reaction in a Teflon-lined autoclave and washed several times with dilute hydrochloric acid and deionized water to obtain MCHRs. Electrochemical measurements revealed that MCHRs had better Na storage performance, higher rate capability, more stable cycling performance and superior reversible specific capacity.[41]

The vertically oxygen-incorporated MoS_2 nanosheets coated on carbon fiber (OMSCF) were synthesized by hydrothermal process and calcination reaction in air. First, carbon fiber was extracted from commercial wet tissue (Vinda Paper Group) with concentrated hydrochloric acid. Second, graphite oxide (GO) was synthesized through the modified Hummers' method. Finally, MoS_2/carbon fibers (MSCF) were obtained by hydrothermal method. The FESEM images of OMSCF are shown in Fig. 3c. Oxygen atoms are incorporated into MoS_2 by the MSCF calcined in air. The incorporation of oxygen not only creates more defects, but also expands the interlayer spacing. The composite of carbon fiber and MoS_2 nanosheets not only improves electronic conductivity, but also enhances structural stability.[43]

In addition, Zhang *et al.*[45] prepared ternary $MoS_{2-x}Se_x$ alloy/graphene ($MoS_{2-x}Se_x$/G) composite though hydrothermal reaction and selenization treatment (Fig. 3d). The interlayer spacing of MoS_2 is expanded due to the doping of Se atoms which facilitates Na^+ fast transfer. Meanwhile, the electronic conductivity of composite is enhanced due to graphene, which boosts the electrochemical performance for NIBs.

Dai *et al.*[44] reported a series of molecule-intercalated MoS_2 as anode materials for SIBs. The molecular intercalation method expands the interlayer spacing as well as increases the electrical

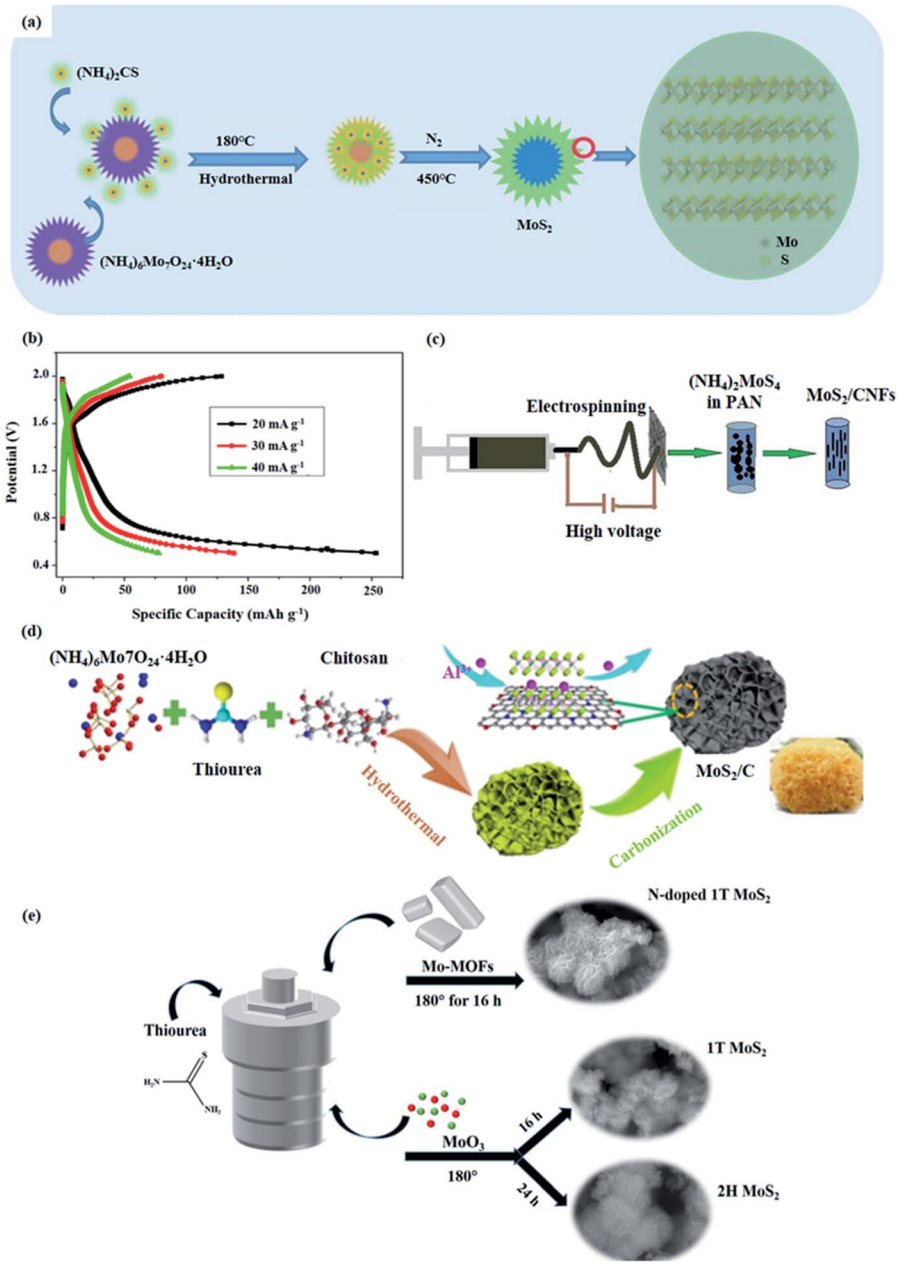

Fig. 4 (a) Schematic illustration of MoS_2 microspheres prepared by hydrothermal method.[47] (b) The first discharge–charge curves at different current densities.[47] (c) Schematic illustration of the preparation process of MoS_2/CNFs.[48] (d) The preparation process of MNC.[49] (e) The synthesis of N-doped 1T MoS_2, pure 1T MoS_2, and 2H MoS_2.[50]

conductivity of MoS_2 (Fig. 3e and f). The interlayer spacing can be varied in the range of 0.62 to 1.26 nm precisely by inserting different molecules (Fig. 3g).

In the example of the dimethylacetamide–MoS_2 (DAM–MoS_2) construct, MoS_2 was synthesized by hydrothermal method firstly. Second, squeezing small DAM molecules into the layers.[46] Specifically, DAM, $(NH_4)_6Mo_7O_{24}\cdot 4H_2O$, $Na_2S\cdot 9H_2O$, $N_2H_4\cdot H_2O$ and deionized water were mixed. Then, the mixture was placed in Teflon-liner autoclave and heated at 230 °C for 24 h. Finally, dark powders were collected after naturally cooled to RT. Benefiting from the expanded interlayer spacing and improved conductivity, the electrochemical performance of SIBs with MoS_2 as the electrode material has been enhanced.

2.3 Other rechargeable batteries

Aluminum ion batteries (AIBs) are also members of energy storage systems. MoS_2 and its composites can be used as cathode materials for AIBs. Li *et al.*[47] prepared MoS_2 microspheres structure by hydrothermal method. The preparation process is shown in the Fig. 4a. First, the MoS_2 microsphere precursor was synthesized by using $(NH_4)_6Mo_7O_{24}\cdot 4H_2O$ and $(NH_4)_2CS$ in a hydrothermal method. And then, MoS_2 microsphere was obtained by heat treatment in a nitrogen atmosphere.

Fig. 4b depicts the electrochemical performance of MoS_2 microspheres. Obviously, the electrochemical performance of AIBs with MoS_2 microsphere cathode material is not excellent. The reason for this can be attributed to the inherent defects of MoS_2. Therefore, future research focusing on enhancing the electrochemical properties of MoS_2 electrode materials is needed.

Yang *et al.*[48] reported a flexible free-standing MoS_2/CNFs cathode for rechargeable AIBs. As shown in Fig. 4c, the MoS_2/CNFs are prepared by electrospinning and annealing treatment. As electrode materials for AIBs, MoS_2/CNFs exhibit better cycling stability and higher rate capacity than MoS_2 microspheres.

In order to overcome the defects of MoS_2 and achieve the improved electrochemical performance of AIBs, another method is to use N-doped carbon materials compounded with MoS_2 as a cathode material for AIBs. Guo *et al.*[49] synthesized interlayer-expanded MoS_2/N-doped carbon (MNC) with a three-dimensional (3D) hierarchical structure by a hydrothermal method and calcination. Fig. 4d represents the synthesis of MNC. Electrochemical test results illustrated that MNC had excellent cycling ability and high discharge capacity, which were owing to the unique 3D structure provides a large specific surface area and the N-doped carbon expands the interlayer spacing of MoS_2.

Aqueous zinc ion batteries (ZIBs) are one of the rechargeable batteries based on divalent cations. Nevertheless, Zn^{2+} has strong interactions with water molecules, increasing the difficulty of Zn^{2+} diffusion and intercalation,[54] which hinders the development of ZIBs. To address these problems, researchers used MoS_2 as an electrode material to improve the electrochemical performance of ZIBs by increasing its interlayer spacing through doping with nitrogen or oxygen.[50,54]

In the example of the N-doped MoS_2, Mo–organic framework (Mo–MOF) served as the nitrogen source. Basing on the one-step hydrothermal sulfurization, N-doped MoS_2 was prepared.[50] Ideally, the 1T and 2H phases of MoS_2 can be obtained by different reaction conditions (Fig. 4e).

The electrochemical test results illustrated that N-doped 1T MoS_2 has not only high multiplicative performance but also superior cycling stability, which greatly improves the electrochemical performance of ZIBs.

In order to better display the synthesis and application of MoS_2-based nanomaterials in electrode materials, the preparation methods and batteries performance are summarized in Table 1. In addition, we also collected some typical nanomaterials for battery applications to compare with MoS_2.[51–53]

3. Applications and synthesis strategies of MoS_2 in catalyst for water splitting

The use of large amounts of fossil fuels has led to increasing environmental degradation, therefore, it is essential to produce clean, renewable energy. Hydrogen energy, as one of the clean energy sources, has been widely researched in recent years. Electrocatalytic water splitting and photocatalytic water splitting are recognized as efficient methods for the preparation of hydrogen.[55–60] The water splitting reaction requires an efficient catalyst. It is well known that MoS_2 is a lamellar structure with abundant active sites at the edges. This property makes it a promising non-precious metal catalyst with large numbers of applications in catalysis. However, the defects of MoS_2 with low bulk conductivity and anisotropic electrical transport restrict the catalytic efficiency. Therefore, researchers have developed amount of MoS_2 composite catalysts to improve the catalytic efficiency.

3.1 Electrocatalyst

According to previous reports, either 1T-phase MoS_2 catalysts or MoS_2 composites catalysts have efficient catalytic performance in the HER. In detail, 1T-phase MoS_2 has higher catalytic performance than 2H-phase MoS_2, benefiting from the fast charge transfer rate in the metal phase.[61] The compounding of MoS_2 with MoN can not only improve the electrical conductivity of MoS_2, but also make MoS_2 have good stability in acidic and alkaline environments.[62] The compounding of MoS_2 with CNFs can improve the electrical conductivity of MoS_2 and restrict the growth of MoS_2 nanosheets.[63] In addition, MoS_2 composites can be used as bifunctional and efficient electrocatalysts for water splitting. For example, CoS_2–C@MoS_2 exhibits both excellent HER catalytic performance and good oxygen evolution reaction (OER) catalytic performance.[64] MoS_2 compounded with Mo_2N-containing multichannel hollow CNFs (Mo_2N–MoS_2 MCNFs) also possesses excellent HER and OER catalytic properties.[65] Subsequently, the preparation of these materials will be described.

1T-MoS_2 was synthesized by hydrothermal reaction. Specifically, $(NH_4)_6Mo_7O_{24}\cdot 4H_2O$ and N_2H_4CS were dissolved in

Table 1 MoS_2-based nanocomposites for electrode materials

No.	Materials	Preparation	Mo source	S source	Morphology of MoS_2	Battery electrodes	Specific capacity (mA h g^{-1})	Cycling number	Current rate (mA g^{-1})	Ref.
1	MoS_2	Wet etching method	$Na_2MoO_4 \cdot 2H_2O$	Sulfur	Nanotube	LIBs cathode	1150	250	200	36
2	MoS_2/C/C	Hydrothermal and electrospinning method	$(NH_4)_6Mo_7O_{24} \cdot 4H_2O$	N_2H_4CS	Sphere	LIBs anode	1062	150	200	34
3	TiO_2/C/MoS_2	Solvent-thermal method and calcination	$(NH_4)_6Mo_7O_{24} \cdot 4H_2O$	N_2H_4CS	Fish-scale-shaped (10 nm in size)	LIBs anode	621	100	100	35
4	MoS_2/C	Template method	$Na_2MoO_4 \cdot 2H_2O$	$N_2H_4C_S$	Nanosheet	SIBs anode	484.9	1500	2000	42
5	MoS_2/CNFs	Electrospinning and high temperature carbonization	AMT	AMT	Single-layer structure	SIBs anode	485	100	100	40
6	MCHRs	One-pot solvothermal reaction	$MoO_2(acac)_2$	N_2H_4CS	Nanosheet	SIBs anode	265	3000	10 000	41
7	OMSCF	Hydrothermal process and calcination reaction	Na_2MoO_4	N_2H_4CS	Nanosheet	SIBs anode	330	100	100	43
8	$MoS_{2-x}Se_x$/G	Hydrothermal reaction and selenization treatment	$(NH_4)_6Mo_7O_{24} \cdot 4H_2O$	N_2H_4CS	—	SIBs anode	178	700	2000	45
9	DAM–MoS_2	Hydrothermal method	$(NH_4)_6Mo_7O_{24} \cdot 4H_2O$	$Na_2S \cdot 9H_2O$	Layered structure (0.62–1.24 nm in size)	SIBs anode	420	600	100	44
10	MoS_2	Hydrothermal method	$(NH_4)_6Mo_7O_{24} \cdot 4H_2O$	N_2H_4CS	Microsphere	AIBs cathode	66.7	100	40	47
11	MoS_2/CNFs	Electrospinning and annealing treatment	$(NH_4)_2MoS_4$	$(NH_4)_2MoS_4$	Nanosheet	AIBs cathode	130	200	100	48
12	MNC	Hydrothermal method and calcination	$(NH_4)_6Mo_7O_{24} \cdot 4H_2O$	N_2H_4CS	Nanosheet	AIBs cathode	127.5	1700	1000	49
13	N-doped MoS_2	One-step hydrothermal sulfurization	Mo–MOF	N_2H_4CS	Nanoflower	ZIBs cathode	98.1	1000	3000	50
14	hBN/C	Liquid-phase shear exfoliation method	—	—	—	LIBs separators	158	100	—	51
15	rGO/Al	Electrospraying	—	—	—	$LiNi_{0.5}Mn_{1.5}O_4$ cathode	109.5	840	—	52
16	$P_4Nb_2O_{15}$@CNTs	Solvothermal method	—	—	—	LIBs anode	250	500	—	53

distilled water to form a homogeneous solution, and then the solution was put into a Teflon-lined stainless steel autoclave for reaction. The formation of 1T phase or 2H phase depends on the reaction temperature.

Hierarchical MoS_2/MoN heterostructures were obtained by a simple hydrothermal reaction and nitridation treatment. MoS_2 nanospheres were synthesized from N_2H_4CS and hexaammonium molybdate in a hydrothermal reaction. Subsequently, the layered MoS_2/MoN heterostructures were synthesized by nitriding under ammonia atmosphere.

MoS_2–carbon CNFs were prepared by electrospinning and graphitization treatment. First, $(NH_4)_2MoS_4$ was dissolved in PAN solution and used for electrospinning to prepare PAN/$(NH_4)_2MoS_4$ (PANAMo) nanofibers. Afterwards, the precursor nanofibers were graphitized to obtain MoS_2–CNFs hybrids.

CoS_2–C@MoS_2 core–shell nanofibers were fabricated by electrospinning method, carbonization treatment and hydrothermal synthesis. First, a certain amount of PAN and $Co(Ac)_2 \cdot 4H_2O$ were dissolved in DMF to prepare $Co(Ac)_2$/PAN membranes by electrospinning method. Later, the Co–C nanofibers were obtained by carbonization under Ar atmosphere. Second, CoS_2–C@MoS_2 core–shell nanofibers were prepared by a simple hydrothermal method using $(NH_4)_2MoS_4$ as the S source.

As depicted in Fig. 5a, the synthesis of Mo_2N–MoS_2 MCNFs was achieved by a four-step procedure. First, a certain amount

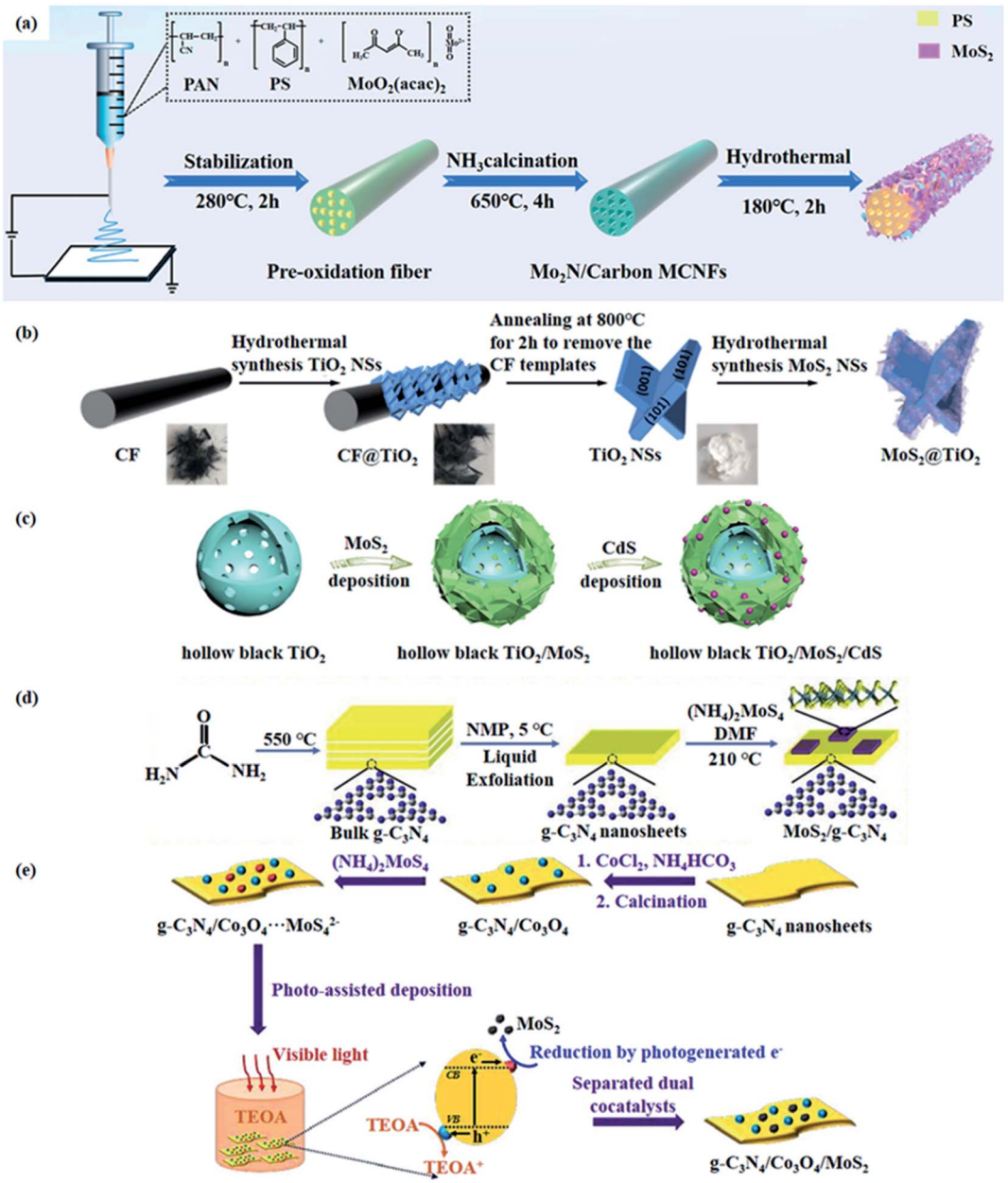

Fig. 5 The diagrammatic sketch for the preparation of (a) Mo_2N–MoS_2 MCNFs,[65] (b) MoS_2@TiO_2 composites,[68] (c) TiO_2/MoS_2/CdS tandem heterojunction,[69] (d) 2D–2D MoS_2/g-C_3N_4 composites[70] and (e) g-C_3N_4/Co_3O_4/MoS_2 heterojunction.[71]

Table 2 MoS_2-based nanocomposites for electrocatalyst and photocatalyst

						Electrocatalyst		
No.	Materials	Preparation	Mo source	S source	Morphology of MoS_2	Tafel slope (mV dec^{-1})	Overpotential (mV *vs.* RHE) at $J = 10$ mA cm^{-2}	Ref.
1	1T-MoS_2	Hydrothermal reaction	$(NH_4)_6Mo_7O_{24}\cdot 4H_2O$	Thiourea	Nanosheet	54 (HER)	214 (HER)	61
2	MoS_2/MoN	Hydrothermal reaction and nitridation treatment	Hexaammonium molybdate	Thiourea	Nanosphere	98 (HER, KOH); 87 (HER, H_2SO_4)	132 (HER, KOH); 117 (HER, H_2SO_4)	62
3	MoS_2/CNFs	Electrospinning and graphitization treatment	$(NH_4)_2MoS_4$	$(NH_4)_2MoS_4$	Nanoplate	42 (HER)	93 (HER)	63
4	CoS_2–C@MoS_2	Electrospinning method, carbonization treatment and hydrothermal synthesis	$(NH_4)_2MoS_4$	$(NH_4)_2MoS_4$	Nanosheet	61 (HER); 46 (OER)	173 (HER); 391 (OER)	64
5	Mo_2N–MoS_2 MCNFs	Electrospinning method, NH_3 calcination and hydrothermal synthesis	$(NH_4)_6Mo_7O_{24}\cdot 4H_2O$	Thiourea	Nanosheet	68.9 (HER); 57.2 (OER)	131 (HER); 270 (OER)	65
6	Graphene–hBN	Exfoliation and Hummer's method	—	—	—	—	390 (HER)	66
7	Cobalt- and nitrogen-codoped graphene	Annealing strategy	—	—	—	73 (OER)	210 (OER)	67

						Photocatalyst	
No.	Materials	Preparation	Mo source	S source	Morphology of MoS_2	H_2 evolution rate (mmol h^{-1} g^{-1})	Ref.
8	MoS_2@TiO_2	Hydrothermal/annealing treatment and subsequent photoreduction method	$(NH_4)_2MoS_4$	$(NH_4)_2MoS_4$	Nanosheet	2.16	68
9	TiO_2/MoS_2/CdS	Template-free solvothermal approach, solvothermal approach and wet chemical method	MoO_3	Thiourea	Nanosheet	9	69
10	MoS_2/g-C_3N_4	Direct heating of urea and a solvent-thermal method	$(NH_4)_2MoS_4$	$(NH_4)_2MoS_4$	Nanosheet	1.155	70
11	g-C_3N_4/Co_3O_4/MoS_2	Two-step thermal treatment, coprecipitation-calcination strategy and *in situ* photo-deposition	$(NH_4)_2MoS_4$	$(NH_4)_2MoS_4$	MoS_2 nanocrystal	5.25	71
12	Sulfur-doped h-BN	CVD	—	—	—	1.3485	72

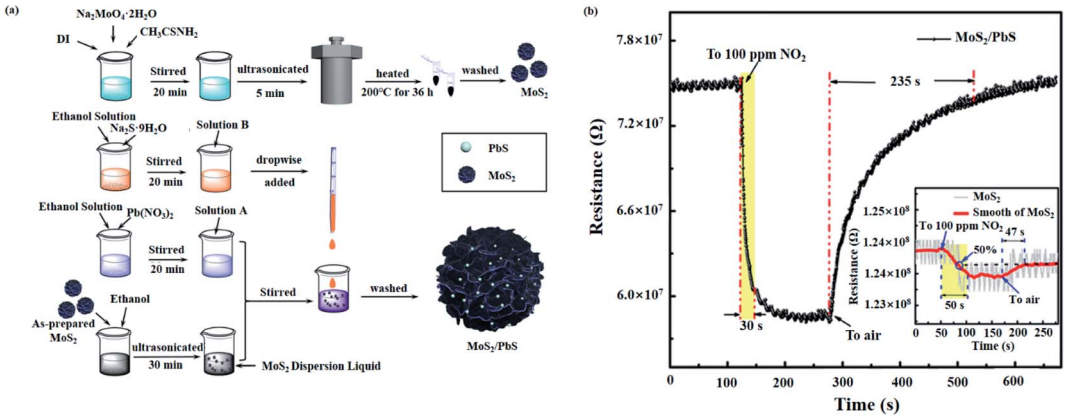

Fig. 6 (a) Preparation process of MoS_2/PbS composites.[78] (b) Transient response characteristic of MoS_2/PbS gas sensor at 100 ppm NO_2.[78]

of PAN and polystyrene (PS) were dissolved in DMF, stirred well and then $MoO_2(acac)_2$ was added to form a precursor solution for electrospinning to obtain $MoO_2(acac)_2$@PAN/PS fiber. Second, previously obtained fiber was pre-oxidized in air. Third, Mo_2N/C MCFs were prepared by calcination of the pre-oxidation fiber under NH_3 atmosphere. During calcination, PS gradually decomposed, leading to the formation of channels in the fibers. Finally, Mo_2N–MoS_2 MCNFs were successfully prepared by

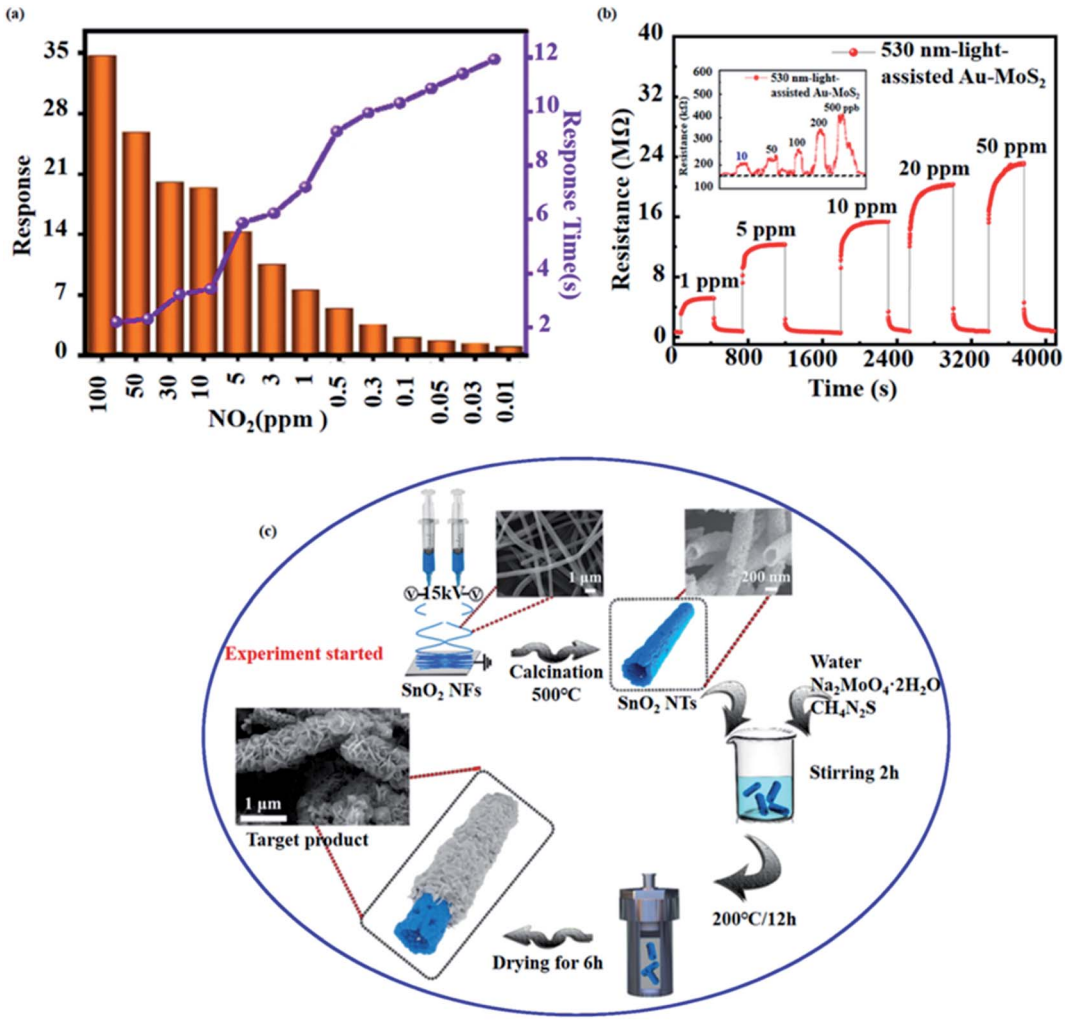

Fig. 7 (a) Response and response time of MoS_2@SnO_2 sensor to 0.01–100 ppm NO_2.[79] (b) Real-time sensing response curves of the 530 nm-light-assisted Au–MoS_2 sensor at 1–50 ppm NO_2.[80] (c) Schematic diagram of the synthesis of MoS_2@SnO_2.[79]

hydrothermal method to grow MoS_2 nanosheets on the surface of Mo_2N/Carbon MCNFs.

3.2 Photocatalyst

Photocatalytic water splitting reaction is considered as one of the effective ways to prepare green, renewable energy, due to its ability to convert solar energy into hydrogen energy. In recent years, with the development of hydrogen preparation reaction by photocatalytic water splitting, more and more photocatalysts have been studied and prepared, including those prepared with graphite carbon nitride (g-C_3N_4), TiO_2 or CdS as materials. It has been shown that the compound of MoS_2 with the above materials can improve the catalytic activity of the photocatalyst and promote the preparation of hydrogen by water splitting.[68–71,73]

Hu *et al.*[68] prepared MoS_2@TiO_2 composites by using combination of hydrothermal/annealing treatment with subsequent photoreduction method. It is noted that MoS_2 nanosheets can be selectively deposited on the (101) facets of TiO_2, allowing for increased photocatalytic hydrogen production activity of the MoS_2@TiO_2 composites. Sun *et al.*[69] fabricated a hollow TiO_2/MoS_2/CdS tandem heterojunction *via* three main steps. First, the hollow mesoporous TiO_2 spheres were synthesized by a template-free solvothermal approach. Second, MoS_2 nanosheets were coated on the surface of TiO_2 by a solvothermal approach. Finally, CdS nanoparticles were selectively deposited on the edges of MoS_2 nanosheets though a wet chemical method. MoS_2 not only serves as an excellent cocatalyst, but also promotes charge separation and effectively inhibits the complexation of photogenerated electrons and holes. Yuan *et al.*[70] obtained 2D–2D MoS_2/g-C_3N_4 photocatalyst though a simple probe sonication assisted liquid exfoliation method and a solvent-thermal method. The large surface area of g-C_3N_4 nanosheets and the large 2D nanointerface between MoS_2 and g-C_3N_4 nanosheets greatly enhance the catalytic hydrogen production activity of the photocatalyst. Zhao *et al.*[71] synthesized g-C_3N_4/Co_3O_4/MoS_2 heterojunction *via* chemical deposition and photo-deposition method. Co_3O_4 and MoS_2 were used as co-catalysts with efficient photocatalytic activity under visible light irradiation. Their synthesis schematic is demonstrated in Fig. 5b–e.

In order to better display the synthesis and application of MoS_2-based nanomaterials in catalysis, the preparation methods and catalytic performance are summarized in Table 2. Furthermore, for comparison, we summarize performance parameters of some typical nanomaterials in electrocatalysis and photocatalysis at the end of the table.[66,67,72]

4. Applications and synthesis strategies of MoS_2 in gas sensors

Important factors affecting the performance of gas sensors have been reported to include specific surface area, semiconductor properties, and redox reaction active sites.[74] As mentioned

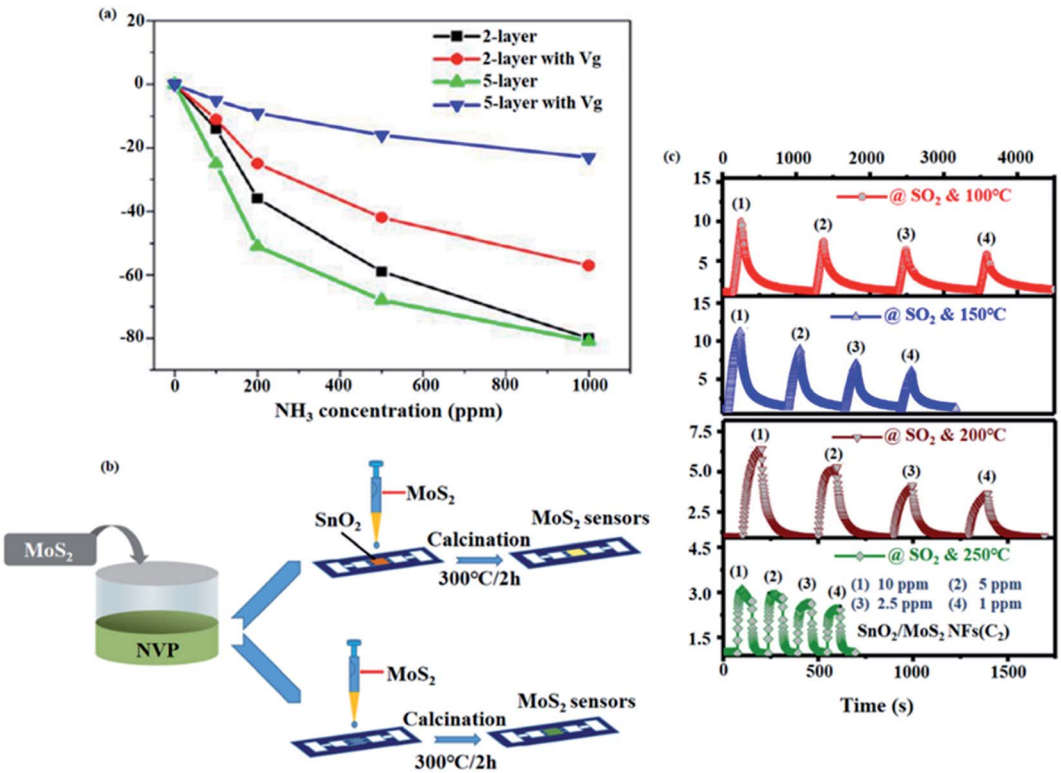

Fig. 8 (a) Sensitivity of 2-layer and 5-layer MoS_2 as a function of NH_3 concentration.[74] (b) Schematic diagram of the fabrication of MoS_2 sensors and MoS_2/SnO_2 sensors.[81] (c) Response of MoS_2/SnO_2 sensors to different concentrations of SO_2 gas at different operating temperatures.[81]

earlier, MoS_2 is a graphene-like material possessing a 2D layer structure with a large specific surface area and excellent semiconductor properties. In addition, it has been pointed out that MoS_2 has different affinities for different molecules,[75] which makes MoS_2 one of the promising materials for the preparation of gas sensors.

4.1 MoS_2-based gas sensors toward nitrogen dioxide

Nitrogen dioxide (NO_2) is one of the prevalent pollutants in the air, as well as a toxic gas that endangers human health, causing great damage to human eyes and respiratory tracts even when exposed to concentrations as low as 3 ppm.[76] Therefore, it is urgent to develop gas sensors that can detect NO_2 effectively and rapidly. The detection of NO_2 by pure MoS_2 or MoS_2 composites as gas-sensitive elements is one of the main focuses of gas sensors research in recent years.

Using pure MoS_2 as gas sensitive element, some researches have prepared MoS_2 by chemical vapor deposition (CVD) method. For instance, Kumar *et al.*[77] obtained 2D MoS_2 by CVD with MoO_3 powder and sulfur as precursors. The test results revealed that the MoS_2 gas sensor had a response time of 29 s and a recovery time of 350 s for 100 ppm concentration of NO_2 when operating in a RT environment irradiated by UV lamps (~365 nm). Similarly, Kim *et al.*[13] fabricated layer-controlled MoS_2 by CVD with molybdenum hexacarbonyl ($Mo(CO)_6$) and hydrogen sulfide (H_2S). It is found that the Schottky barrier changes due to the change in the number of MoS_2 layers, which results in an improved response of the gas sensor. Zheng *et al.*[75] synthesized n-type and p-type MoS_2 films by CVD and soft-chemistry route, respectively. In CVD process, MoO_3 and sulfur were used as precursors, while in the soft-chemistry route, molybdate sol–gel (contain 1% W) was used as precursors. Uniquely, they prepared a novel p–n junction gas sensor by stacking n-type and p-type MoS_2 atomic layers. The results represented that compared with n-type MoS_2 gas sensor, the p-type MoS_2 has a faster response to NO_2. More importantly, the p–n junction sensor not only has a 20-fold increase in sensitivity to 20 ppm NO_2, but also has a lower detection limit of 8 ppb.

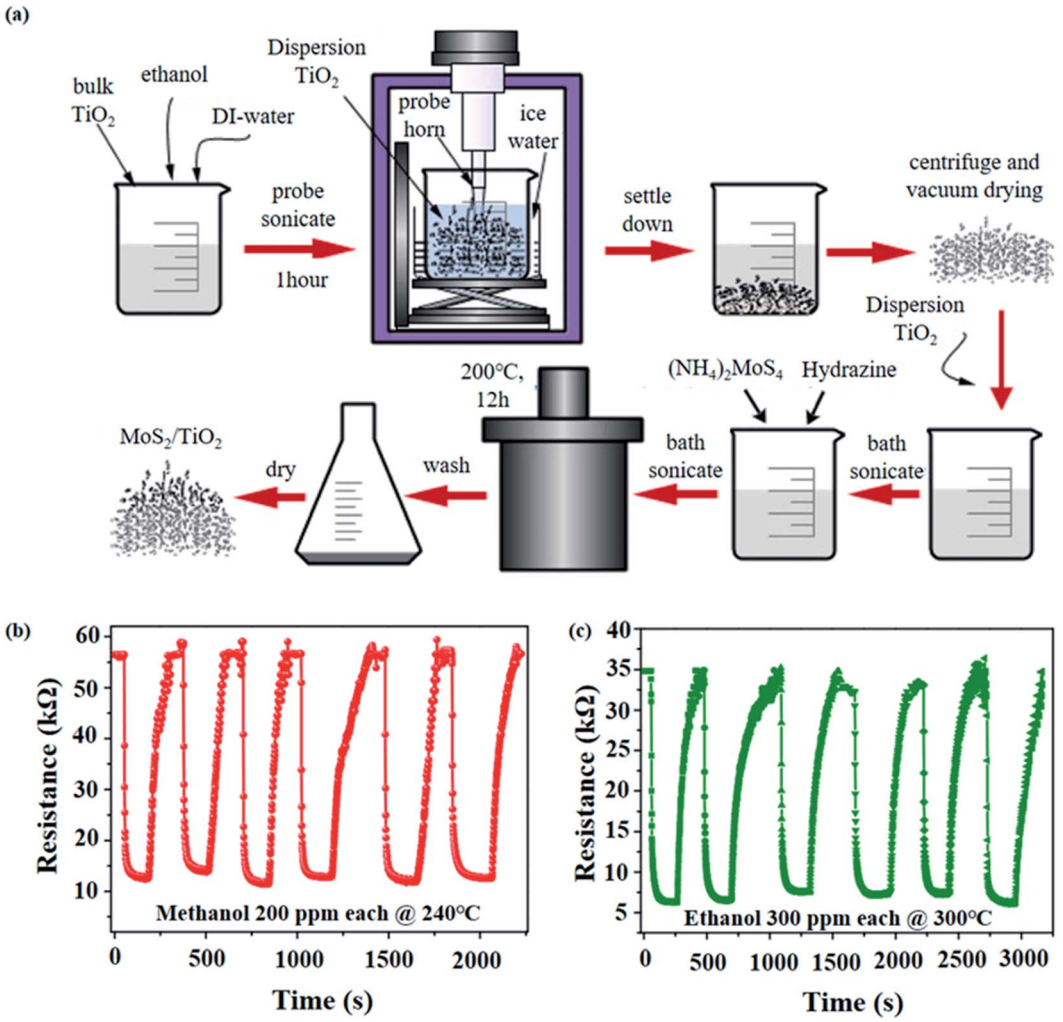

Fig. 9 (a) Schematic diagram of the synthesis of MoS_2/TiO_2 composite.[82] (b) Repeatability testing of 200 ppm methanol for six consecutive cycles at an operating temperature of 240 °C.[82] (c) Repeatability testing of 300 ppm methanol for six consecutive cycles at an operating temperature of 300 °C.[82]

Table 3 MoS_2-based nanocomposites for gas sensors

No.	Materials	Preparation	Mo source	S source	Morphology	Target Gas	Res/Rec (s)	Response (R_g/R_a)	T (°C)	Detection limits	Ref.
1	MoS_2	CVD	MoO_3	Sulfur	Film	100 ppm of NO_2	29/350	1.3516	RT (UV)	—	77
2	MoS_2	CVD	$Mo(CO)_6$	H_2S	Film	10 ppm of NO_2	—/—	1.6	RT	—	13
3	MoS_2	CVD	MoO_3	Sulfur	Film	20 ppm of NO_2	150/30	—	RT (UV)	8 ppb	75
4	MoS_2/PbS	Hydrothermal method combined with chemical precipitation	$Na_2MoO_4 \cdot 2H_2O$	CH_3CSNH_2	Fluffy ball-like structure	100 ppm of NO_2	30/235	—	RT	—	78
5	MoS_2@SnO_2	Electrospinning and hydrothermal growth	$Na_2MoO_4 \cdot 2H_2O$	N_2H_4CS	Nanoflake	100 ppm of NO_2	2.2/10.54	0.02884	RT	10 ppb	79
6	Au–MoS_2	Hydrothermal method	$Na_2MoO_4 \cdot 2H_2O$	CH_3CSNH_2	Fluffy flower-like structure	1 ppm of NO_2	—/27	8.1	RT (530 nm LED)	10 ppb	80
7	MoS_2	Micromechanical exfoliation method	Bulk MoS_2 crystal	Bulk MoS_2 crystal	Layered	1000 ppm of NO_2	—/—	14.72	RT	—	74
8	MoS_2	Micromechanical exfoliation method	Bulk MoS_2 crystal	Bulk MoS_2 crystal	Layered	1000 ppm of NH_3	—/—	1.86	RT	—	74
9	SnO_2/MoS_2	Electrospinning and drop-coated process	MoS_2 powder	MoS_2 powder	Nanosheet	10 ppm of SO_2	—/—	11.1	150	5 ppt (parts-per-trillion)	81
10	MoS_2/TiO_2	Low-cost hydrothermal method	$(NH_4)_2MoS_4$	$(NH_4)_2MoS_4$	Layered	500 ppm of ethanol	50/100	nearly 0	300	—	82
11	MoS_2/TiO_2	Low-cost hydrothermal method	$(NH_4)_2MoS_4$	$(NH_4)_2MoS_4$	Layered	500 ppm of methanol	—/—	0.15	240	—	82
12	CuO/rGO	LbL self-assemble	—	—	—	1 ppm of CO	70/160	1.0256	RT	—	83
13	Single-walled carbon nanotubes	—	—	—	—	100 ppb of NO	—/—	0.7136	RT	—	84
14	Graphene oxide	Thermal reduction	—	—	—	5 ppm of NO_2	—/—	0.83	RT	—	85
15	DETA doped graphene	CVD and vapor-phase molecular doping	—	—	—	50 ppm of NO_2	—/—	0.23	RT	0.83 ppq (parts per quadrillion)	86

Just as pure MoS_2 gas sensors exhibit gas-sensitive performance on NO_2 gas, MoS_2 composite gas sensors also have excellent gas-sensitive properties. For example, the PbS quantum dots modified MoS_2 (MoS_2/PbS) composite gas sensor prepared by Xin *et al.*[78] has excellent gas-sensitive performance for NO_2 due to the high response of PbS quantum dots to NO_2 and the prevention of MoS_2 oxidation. MoS_2/PbS was prepared by hydrothermal and chemical precipitation methods, and the specific preparation is shown in Fig. 6a. First of all, pure MoS_2 was prepared from $Na_2MoO_4 \cdot 2H_2O$ and CH_3CSNH_2 by hydrothermal reaction under an Teflon-lined autoclave at 200 °C. Secondly, the doping of PbS quantum dots was achieved by chemical precipitation using $Na_2S \cdot 9H_2O$ and $Pb(NO_3)_2$ as precursors. Compared with pure MoS_2, the MoS_2/PbS gas sensor has higher response and recovery performance for 100 ppm NO_2 gas at RT (Fig. 6b).

Composites of MoS_2 nanosheets with SnO_2 nanotubes were prepared for gas-sensitive properties by Bai *et al.* MoS_2@SnO_2 heterostructure exhibits impressive sensitivity and selectivity for the detection of NO_2 gas at RT. Tests illustrated that the MoS_2@SnO_2 gas sensor had a fast response time (2.2 s), a short recovery time (10.54 s), a low detection limit (10 ppb) and excellent stability (20 weeks) (Fig. 7a).[79] Another reported composite is MoS_2 nanoflowers modified with Au nanoparticles prepared by Chen *et al.* Surprisingly, the Au–MoS_2 gas sensor exhibits an extremely low detection limit (10 ppb) for NO_2 at RT with strong resistance to moisture interference under 530 nm light illumination (Fig. 7b).[80]

The preparation of MoS_2@SnO_2 was achieved by electrostatic spinning and hydrothermal methods, as presented in Fig. 7c. First, stannous chloride ($SnCl_2 \cdot 2H_2O$) was mixed with anhydrous ethanol, DMF and PVP to make electrospinning solution, and SnO_2 NTs were obtained by spinning technique and subsequent high-temperature calcination treatment. Second, N_2H_4CS and $Na_2MoO_4 \cdot 2H_2O$ were used as the S and Mo sources, respectively, to mix with the previously prepared SnO_2 NTs, and the reaction was carried out in an autoclave at 200 °C to realize MoS_2 on SnO_2 NTs growth.[79]

The fabrication of Au–MoS_2 composites was achieved by a two-step hydrothermal method. Firstly, MoS_2 was obtained by reacting $Na_2MoO_4 \cdot 2H_2O$ and thioacetamide (CH_3CSNH_2) in a Teflon-lined autoclave at 200 °C for 36 h. Secondly, Au–MoS_2 was synthesized by mixing sodium citrate tribasic dihydrate ($C_6H_5Na_3O_7 \cdot 2H_2O$), tannic acid ($C_{76}H_{52}O_{46}$) and previously prepared MoS_2, then adding gold chloride trihydrate ($HAuCl_4 \cdot 3H_2O$) solution dropwise and stirring well, and then reacting in a Teflon-lined autoclave.[80]

4.2 MoS_2-based gas sensors for other gases

The MoS_2-based gas sensors not only detect NO_2 gas extremely well, but also reveal excellent gas sensitivity to NH_3, SO_2 and alcohol gases.

Dattatray J. Late *et al.*[74] prepared layered MoS_2 films by micromechanical exfoliation method in 2013 for the preparation of gas sensors to detect NH_3 gas. The experimental results demonstrated that the 2-layer MoS_2 and 5-layer MoS_2 have excellent gas-sensitive performance to NH_3, and the 5-layer MoS_2 is more sensitive to detect NH_3. In addition, when the MoS_2 gas sensor is applied with a positive gate voltage, the electric field formed at the interface will repel the electrons given by NH_3 as an electron donor, resulting in a decrease in the sensitivity of MoS_2 to NH_3. Fig. 8a shows the curves of sensitivity with NH_3 concentration for 2-layer and 5-layer MoS_2 with and without gate voltage.

Nguyen Ngoc Viet *et al.*[81] prepared MoS_2/SnO_2 sensors for SO_2 gas detection by on-chip electrostatic spinning and subsequently dropping MoS_2 nanosheets-dispersed solution, and the fabrication is depicted in Fig. 8b. The test results indicated that the MoS_2/SnO_2 gas sensor had good gas-sensitive performance for 10 ppm SO_2 gas at 150 °C (Fig. 8c).

Sukhwinder Singh *et al.*[82] prepared MoS_2/TiO_2 composite for the detection of methanol and ethanol. As shown in Fig. 9a, MoS_2/TiO_2 hybrid was obtained by two steps: first, pure TiO_2 powder was mixed with ethanol and other solvents for probe sonication, and second, $(NH_4)_2MoS_4$ was mixed with the produced TiO_2 suspension to prepare MoS_2/TiO_2 composites by hydrothermal method. The test results revealed that the best working temperatures of MoS_2/TiO_2 composites for methanol and ethanol were 240 °C and 300 °C, respectively, and more importantly, the MoS_2/TiO_2 sensor had good response and better stability (Fig. 9b and c).

The gas sensing performance of MoS_2-based nanomaterials and the preparation methods are listed in Table 3. As a comparison, the gas-sensitive properties of some typical materials are collected at the end of the table.[83–86]

5. Conclusion

This review highlights recent advances in MoS_2-based materials synthesis and their applications toward batteries, catalysts and gas sensors. First of all, MoS_2, due to the large specific surface area and abundant active sites, has become one of the most popular electrode materials. In addition, the compound of MoS_2 with CNFs and TiO_2 materials overcomes the inherent defects of MoS_2 and greatly improves the electrochemical performance of the battery. Second, MoS_2 has catalytic active sites on the edges, which makes it one of the most popular candidates to replace noble metal catalysts. The composite of MoS_2 with MoN, CoS_2 and C_3N_4 improved the catalytic performance of the catalyst. Finally, MoS_2 can be used in gas sensors due to the semiconductor properties and non-zero forbidden bandwidth. The compound of MoS_2 with materials such as SnO_2 and PbS can enhance the sensitivity of the gas sensor to the gas to be detected and reduce the detection limit.

It is worth noting that while MoS_2 has made good progress in these areas, challenges remain in its future development. First, MoS_2 has low electrical conductivity and multilayer MoS_2 tends to accumulate and aggregate in the preparation, which is not conducive to electron transport. Second, the active sites of MoS_2 are mainly at the edges but not at the basal plane, which has a significant impact on both the sensing performance and catalytic performance. Therefore, it is necessary to further explore the compounding of MoS_2 with other materials or to

optimize the structure of MoS_2 (*e.g.*, preparation of MoS_2 NTs, *etc.*). In addition, 1T-MoS_2 has better electrical conductivity compared with 2H-MoS_2, and there are also interesting electrical properties using 1T-MoS_2 compounded with other materials.

In a word, MoS_2 has promising applications in energy and gas sensors due to its excellent and unique physicochemical properties. We believe that with the joint efforts of researchers in the future, better progress will be made in the applications and synthesis of MoS_2.

Conflicts of interest

There are no conflicts to declare.

Acknowledgements

This work was supported by the National Science Foundation of China (No. 61904123), the Natural Science Foundation of Tianjin (No. 18JCQNJC71800), Scientific Research Project of Tianjin Educational Committee (No. 2018KJ220), Tianjin Technical and Engineering Center of Nonwovens (No. KF202103).

References

1 K. S. Novoselov, D. Jiang, F. Schedin, T. Booth, V. Khotkevich, S. Morozov and A. K. Geim, *Proc. Natl. Acad. Sci.*, 2005, **102**, 10451–10453.
2 S. Z. Butler, S. M. Hollen, L. Cao, Y. Cui, J. A. Gupta, H. R. Gutiérrez, T. F. Heinz, S. S. Hong, J. Huang and A. F. Ismach, *ACS Nano*, 2013, **7**, 2898–2926.
3 G. R. Bhimanapati, Z. Lin, V. Meunier, Y. Jung, J. Cha, S. Das, D. Xiao, Y. Son, M. S. Strano and V. R. Cooper, *ACS Nano*, 2015, **9**, 11509–11539.
4 Z. Wang and B. Mi, *Environ. Sci. Technol.*, 2017, **51**, 8229–8244.
5 H. Wang, C. Li, P. Fang, Z. Zhang and J. Z. Zhang, *Chem. Soc. Rev.*, 2018, **47**, 6101–6127.
6 U. Krishnan, M. Kaur, K. Singh, M. Kumar and A. Kumar, *Superlattices Microstruct.*, 2019, **128**, 274–297.
7 T. Nawz, A. Safdar, M. Hussain, D. Sung Lee and M. Siyar, *Crystals*, 2020, 10.
8 D. Saha and P. Kruse, *J. Electrochem. Soc.*, 2020, 167.
9 O. Samy and A. El Moutaouakil, *Energies*, 2021, 14.
10 Y. Zhang, H. Tao, S. Du and X. Yang, *ACS Appl. Mater. Interfaces*, 2019, **11**, 11327–11337.
11 R. Bose, Z. Jin, S. Shin, S. Kim, S. Lee and Y. S. Min, *Langmuir*, 2017, **33**, 5628–5635.
12 Y. Wang, J. Sunarso, F. Wang, B. Zhao, X. Liu and G. Chen, *Ceram. Int.*, 2017, **43**, 11028–11033.
13 Y. Kim, S. K. Kang, N. C. Oh, H. D. Lee, S. M. Lee, J. Park and H. Kim, *ACS Appl. Mater. Interfaces*, 2019, **11**, 38902–38909.
14 Z. Liu, L. Zhao, Y. Liu, Z. Gao, S. Yuan, X. Li, N. Li and S. Miao, *Appl. Catal., B*, 2019, **246**, 296–302.
15 E. Singh, K. S. Kim, G. Y. Yeom and H. S. Nalwa, *ACS Appl. Mater. Interfaces*, 2017, **9**, 3223–3245.
16 X. Li and H. Zhu, *J. Materiomics*, 2015, **1**, 33–44.
17 Y. Qiao, T. Hirtz, F. Wu, G. Deng, X. Li, Y. Zhi, H. Tian, Y. Yang and T.-L. Ren, *ACS Appl. Electron. Mater.*, 2019, **2**, 346–370.
18 Y. Liu and F. Gu, *Nanoscale Adv.*, 2021, **3**, 2117–2138.
19 O. Samy, S. Zeng, M. D. Birowosuto and A. El Moutaouakil, *Crystals*, 2021, 11.
20 Y. P. Venkata Subbaiah, K. J. Saji and A. Tiwari, *Adv. Funct. Mater.*, 2016, **26**, 2046–2069.
21 W. Zhang, P. Zhang, Z. Su and G. Wei, *Nanoscale*, 2015, **7**, 18364–18378.
22 H. S. Nalwa, *RSC Adv.*, 2020, **10**, 30529–30602.
23 S. Barua, H. S. Dutta, S. Gogoi, R. Devi and R. Khan, *ACS Appl. Nano Mater.*, 2017, **1**, 2–25.
24 S. Shi, Z. Sun and Y. H. Hu, *J. Mater. Chem. A*, 2018, **6**, 23932–23977.
25 L. Lei, D. Huang, G. Zeng, M. Cheng, D. Jiang, C. Zhou, S. Chen and W. Wang, *Coord. Chem. Rev.*, 2019, **399**, 213020.
26 Y. Jiao, A. M. Hafez, D. Cao, A. Mukhopadhyay, Y. Ma and H. Zhu, *Small*, 2018, **14**, e1800640.
27 J. Sun, X. Li, W. Guo, M. Zhao, X. Fan, Y. Dong, C. Xu, J. Deng and Y. Fu, *Crystals*, 2017, 7(7), 198.
28 Z. Liu, X. Wang, Z. Liu, S. Zhang, Z. Lv, Y. Cui, L. Du, K. Li, G. Zhang, M. C. Lin and H. Du, *ACS Appl. Mater. Interfaces*, 2021, **13**, 28164–28170.
29 N. Qiu, Z. Yang, R. Xue, Y. Wang, Y. Zhu and W. Liu, *Nano Lett.*, 2021, **21**, 2738–2744.
30 S. G. Stolyarova, A. A. Kotsun, Y. V. Shubin, V. O. Koroteev, P. E. Plyusnin, Y. L. Mikhlin, M. S. Mel'gunov, A. V. Okotrub and L. G. Bulusheva, *ACS Appl. Energy Mater.*, 2020, **3**, 10802–10813.
31 Z. Yuan, L. Wang, D. Li, J. Cao and W. Han, *ACS Nano*, 2021, **15**, 7439–7450.
32 C. Zhu, X. Mu, P. A. van Aken, Y. Yu and J. Maier, *Angew. Chem., Int. Ed. Engl.*, 2014, **53**, 2152–2156.
33 C.-Y. Wei, P.-C. Lee, C.-W. Tsao, L.-H. Lee, D.-Y. Wang and C.-Y. Wen, *ACS Appl. Energy Mater.*, 2020, **3**, 7066–7072.
34 H. Wu, C. Hou, G. Shen, T. Liu, Y. Shao, R. Xiao and H. Wang, *Nano Res.*, 2018, **11**, 5866–5878.
35 J. Zhang, Y. Li, T. Gao, X. Sun, P. Cao and G. Zhou, *Ceram. Int.*, 2018, **44**, 8550–8555.
36 X. Zhao, Z. Liu, W. Xiao, H. Huang, L. Zhang, Y. Cheng and J. Zhang, *ACS Appl. Nano Mater.*, 2020, **3**, 7580–7586.
37 S. Ding, D. Zhang, J. S. Chen and X. W. Lou, *Nanoscale*, 2012, **4**, 95–98.
38 Y. Lu, X. Yao, J. Yin, G. Peng, P. Cui and X. Xu, *RSC Adv.*, 2015, **5**, 7938–7943.
39 K. Yao, Z. Xu, J. Huang, M. Ma, L. Fu, X. Shen, J. Li and M. Fu, *Small*, 2019, **15**, e1805405.
40 A. Cheng, H. Zhang, W. Zhong, Z. Li, Y. Tang and Z. Li, *J. Electroanal. Chem.*, 2019, **843**, 31–36.
41 L. Han, S. Wu, Z. Hu, M. Chen, J. Ding, S. Wang, Y. Zhang, D. Guo, L. Zhang, S. Cao and S. Chou, *ACS Appl. Mater. Interfaces*, 2020, **12**, 10402–10409.
42 Q. Pan, Q. Zhang, F. Zheng, Y. Liu, Y. Li, X. Ou, X. Xiong, C. Yang and M. Liu, *ACS Nano*, 2018, **12**, 12578–12586.

43 Y. Zhang, H. Tao, T. Li, S. Du, J. Li, Y. Zhang and X. Yang, *ACS Appl. Mater. Interfaces*, 2018, **10**, 35206–35215.
44 H. Dai, M. Tang, J. Huang and Z. Wang, *ACS Appl. Mater. Interfaces*, 2021, **13**, 10870–10877.
45 Y. Zhang, H. Tao, S. Du and X. Yang, *ACS Appl. Mater. Interfaces*, 2019, **11**, 11327–11337.
46 H. Dai, J. Sun, Y. Zhou, Z. Zhou, W. Luo, G. Wei and H. Deng, *ACS Sustainable Chem. Eng.*, 2020, **8**, 8102–8110.
47 Z. Li, B. Niu, J. Liu, J. Li and F. Kang, *ACS Appl. Mater. Interfaces*, 2018, **10**, 9451–9459.
48 W. Yang, H. Lu, Y. Cao, B. Xu, Y. Deng and W. Cai, *ACS Sustainable Chem. Eng.*, 2019, **7**, 4861–4867.
49 S. Guo, H. Yang, M. Liu, X. Feng, H. Xu, Y. Bai and C. Wu, *ACS Appl. Energy Mater.*, 2021, **4**, 7064–7072.
50 Z. Sheng, P. Qi, Y. Lu, G. Liu, M. Chen, X. Gan, Y. Qin, K. Hao and Y. Tang, *ACS Appl. Mater. Interfaces*, 2021, **13**, 34495–34506.
51 A. C. M. de Moraes, W. J. Hyun, N. S. Luu, J. M. Lim, K. Y. Park and M. C. Hersam, *ACS Appl. Mater. Interfaces*, 2020, **12**, 8107–8114.
52 G. Zhang, K. Lin, X. Qin, L. Zhang, T. Li, F. Lv, Y. Xia, W. Han, F. Kang and B. Li, *ACS Appl. Mater. Interfaces*, 2020, **12**, 37034–37046.
53 P. Hei, S. Luo, K. Wei, J. Zhou, Y. Zhao and F. Gao, *ACS Sustainable Chem. Eng.*, 2020, **9**, 216–223.
54 H. Liang, Z. Cao, F. Ming, W. Zhang, D. H. Anjum, Y. Cui, L. Cavallo and H. N. Alshareef, *Nano Lett.*, 2019, **19**, 3199–3206.
55 L. Jia, B. Liu, Y. Zhao, W. Chen, D. Mou, J. Fu, Y. Wang, W. Xin and L. Zhao, *J. Mater. Sci.*, 2020, **55**, 16197–16210.
56 D. Wang, X. Zhang, S. Bao, Z. Zhang, H. Fei and Z. Wu, *J. Mater. Chem. A*, 2017, **5**, 2681–2688.
57 X. Han, X. Tong, X. Liu, A. Chen, X. Wen, N. Yang and X.-Y. Guo, *ACS Catal.*, 2018, **8**, 1828–1836.
58 Y.-J. Yuan, P. Wang, Z. Li, Y. Wu, W. Bai, Y. Su, J. Guan, S. Wu, J. Zhong, Z.-T. Yu and Z. Zou, *Appl. Catal., B*, 2019, **242**, 1–8.
59 X.-L. Yin, G.-Y. He, B. Sun, W.-J. Jiang, D.-J. Xue, A.-D. Xia, L.-J. Wan and J.-S. Hu, *Nano Energy*, 2016, **28**, 319–329.
60 Q. Li, W. Liu, L. Xiao, X. Chen and X. Xu, *Mater. Lett.*, 2021, 285.
61 J. Wang, W. Fang, Y. Hu, Y. Zhang, J. Dang, Y. Wu, H. Zhao and Z. Li, *Catal. Sci. Technol.*, 2020, **10**, 154–163.
62 A. Wu, Y. Gu, Y. Xie, H. Yan, Y. Jiao, D. Wang and C. Tian, *J. Alloys Compd.*, 2021, 867.
63 H. Zhu, F. Lyu, M. Du, M. Zhang, Q. Wang, J. Yao and B. Guo, *ACS Appl. Mater. Interfaces*, 2014, **6**, 22126–22137.
64 Y. Zhu, L. Song, N. Song, M. Li, C. Wang and X. Lu, *ACS Sustainable Chem. Eng.*, 2019, **7**, 2899–2905.
65 D. Xie, G. Yang, D. Yu, Y. Hao, S. Han, Y. Cheng, F. Hu, L. Li, H. Wei, C. Ji and S. Peng, *ACS Sustainable Chem. Eng.*, 2020, **8**, 14179–14189.
66 S. Bawari, N. M. Kaley, S. Pal, T. V. Vineesh, S. Ghosh, J. Mondal and T. N. Narayanan, *Phys. Chem. Chem. Phys.*, 2018, **20**, 15007–15014.
67 Q. Zhang, Z. Duan, M. Li and J. Guan, *Chem. Commun.*, 2020, **56**, 794–797.
68 X. Hu, S. Lu, J. Tian, N. Wei, X. Song, X. Wang and H. Cui, *Appl. Catal., B*, 2019, **241**, 329–337.
69 B. Sun, W. Zhou, H. Li, L. Ren, P. Qiao, W. Li and H. Fu, *Adv. Mater.*, 2018, **30**, e1804282.
70 Y.-J. Yuan, Z. Shen, S. Wu, Y. Su, L. Pei, Z. Ji, M. Ding, W. Bai, Y. Chen, Z.-T. Yu and Z. Zou, *Appl. Catal., B*, 2019, **246**, 120–128.
71 H. Zhao, Z. Jiang, K. Xiao, H. Sun, H. S. Chan, T. H. Tsang, S. Yang and P. K. Wong, *Appl. Catal., B*, 2021, 280.
72 G. Zhao, A. Wang, W. He, Y. Xing and X. Xu, *Adv. Mater. Interfaces*, 2019, **6**, 1900062.
73 N. Qin, J. Xiong, R. Liang, Y. Liu, S. Zhang, Y. Li, Z. Li and L. Wu, *Appl. Catal., B*, 2017, **202**, 374–380.
74 D. J. Late, Y. K. Huang, B. Liu, J. Acharya, S. N. Shirodkar, J. Luo, A. Yan, D. Charles, U. V. Waghmare and V. P. Dravid, *ACS Nano*, 2013, **7**, 4879–4891.
75 W. Zheng, Y. Xu, L. Zheng, C. Yang, N. Pinna, X. Liu and J. Zhang, *Adv. Funct. Mater.*, 2020, **30**, 2000435.
76 T. Pham, G. Li, E. Bekyarova, M. E. Itkis and A. Mulchandani, *ACS Nano*, 2019, **13**, 3196–3205.
77 R. Kumar, N. Goel and M. Kumar, *ACS Sens.*, 2017, **2**, 1744–1752.
78 X. Xin, Y. Zhang, X. Guan, J. Cao, W. Li, X. Long and X. Tan, *ACS Appl. Mater. Interfaces*, 2019, **11**, 9438–9447.
79 X. Bai, H. Lv, Z. Liu, J. Chen, J. Wang, B. Sun, Y. Zhang, R. Wang and K. Shi, *J. Hazard. Mater.*, 2021, **416**, 125830.
80 P. Chen, J. Hu, M. Yin, W. Bai, X. Chen and Y. Zhang, *ACS Appl. Nano Mater.*, 2021, **4**, 5981–5991.
81 N. N. Viet, L. V. Thong, T. K. Dang, P. H. Phuoc, N. H. Chien, C. M. Hung, N. D. Hoa, N. Van Duy, N. Van Toan, N. T. Son and N. Van Hieu, *Anal. Chim. Acta*, 2021, **1167**, 338576.
82 S. Singh and S. Sharma, *Sens. Actuators, B*, 2022, 350.
83 D. Zhang, C. Jiang, J. Liu and Y. Cao, *Sens. Actuators, B*, 2017, **247**, 875–882.
84 D.-W. Jeong, K. H. Kim, B. S. Kim and Y. T. Byun, *Appl. Surf. Sci.*, 2021, 550.
85 Y. R. Choi, Y.-G. Yoon, K. S. Choi, J. H. Kang, Y.-S. Shim, Y. H. Kim, H. J. Chang, J.-H. Lee, C. R. Park, S. Y. Kim and H. W. Jang, *Carbon*, 2015, **91**, 178–187.
86 B. Kwon, H. Bae, H. Lee, S. Kim, J. Hwang, H. Lim, J. H. Lee, K. Cho, J. Ye, S. Lee and W. H. Lee, *ACS Nano*, 2022, **16**, 2176–2187.